Deficient macrophage autophagy protects mice from Cerium Oxide nanoparticle-induced lung fibrosis

Balasubramanyam Annangi
INSERM
Zhuyi Lu
INSERM U955
Jonathan Bruniaux
INSERM U955
Audrey Ridoux
INSERM U955
Vanessa Marques da Silva
INSERM U955
Delphine Vantelon
Synchrotron SOLEIL
Jorge Boczkowski
INSERM U955
Sophie Lanone (sophie.lanone@inserm.fr)
"INSERM" https://orcid.org/0000-0003-2509-8799

Research

Keywords: alveolar fibrosis, autophagy, macrophage polarization, nanoparticle

Posted Date: July 16th, 2020

DOI: https://doi.org/10.21203/rs.3.rs-41389/v1

Version of Record: A version of this preprint was published on February 1st, 2021. See the published version at https://doi.org/10.1186/s12989-021-00398-y.

Abstract

Background

Cerium (Ce) is a rare earth element, rapidly oxidizing to form CeO_2, and currently used in numerous commercial applications, especially as nanoparticles (NP). The potential health effects of Ce remain uncertain, but literature indicates the development of rare earth pneumoconiosis accompanied with granuloma formation, interstitial fibrosis and inflammation. The exact underlying mechanisms are yet not completely understood, and we propose that autophagy could be an interesting target to study, particularly in macrophages. Therefore, the objective of our study was to investigate the role of macrophagic autophagy after pulmonary exposure to CeO_2 NP in mice. Mice lacking the early autophagy gene *Atg5* in their myeloid lineage and their wildtype counterparts were exposed to CeO_2 NP by single oropharyngeal administration and sacrificed up to one month after. At that time, lung remodeling was thoroughly characterized (inflammatory cells infiltration, expression of fibrotic markers such as αSMA, TGFβ1, total and type I and III collagen deposition), as well as macrophage infiltration (quantification and M1/M2 phenotype).

Results:

Such pulmonary exposure to CeO_2 NP induces a progressive and dose-dependent lung fibrosis in the bronchiolar and alveolar walls, together with the activation of autophagy. Blockade of macrophagic autophagy protects from alveolar but not bronchiolar fibrosis, via the modulation of macrophage polarization towards M2 phenotype.

Conclusion:

In conclusion, our findings bring novel insight on the role of macrophagic autophagy in lung fibrogenesis, and add to the current awareness of pulmonary macrophages as potential new therapeutic targets for future anti-fibrotic therapies.

Background

Up to recent years, rare earth elements (REE) received limited attention from environmental and public health researchers. In the last two decades, they have however undergone a fantastic boost in their technological and industrial utilization, which is accompanied by concerns regarding emissions and potential human exposures. One of the main REE currently used in numerous commercial applications is Cerium (Ce), as Ce is very reactive and is a strong oxidizing agent, rapidly oxidizing when in contact with oxygen to form CeO_2. Ce is for example used in flat screen display, alloys, petroleum refining (cracking catalyst), ceramics, glass additives, phosphors, or polishing compounds for glass mirrors, plate glass, television tubes, ophthalmic lenses, precision optics, electronic wafers (1).CeO_2 is also used as additive in cigarettes, and CeO_2 nanoparticles (NP) are predominantly used as diesel fuel additive to increase fuel

combustion efficiency (2). Because of these already numerous current and foreseen applications, CeO_2 NP might enter the environment through disposal of consumer and industrial products, and this is accompanied a growing concern for human health.

The potential health effects of Ce remain uncertain, but RE pneumoconiosis accompanied with granuloma and interstitial fibrosis has been reported in workers exposed to asbestos and RE dusts, together with the presence of Ce-containing particle in macrophages from bronchoalveolar lavage (BAL) and in interstitial macrophages (3, 4). Experimental studies conducted in mice or rats have shown that animal exposure to CeO_2 NP lead to the development of pulmonary fibrosis, accompanied by a persistent pulmonary inflammation and the presence of oxidative stress (1, 5–9). The exact underlying mechanisms are yet not completely understood, and we propose that autophagy could be an interesting target to study.

Autophagy is a physiological process mainly responsible for the recycling of damaged cellular organelles and/or macromolecules into simpler forms for cell survival. The resulting degradation products are recycled to maintain nutrient and energy homeostasis (10, 11). Apart from its importance in physiological conditions, numerous studies have suggested that autophagy is regulated under different pathophysiological conditions, in particular in the lung fibrotic process (12, 13). We have recently demonstrated that macrophagic autophagy can be modulated after exposure to NP, which could be of relevance in the context of pulmonary response to Ce exposure (14).

Therefore, the objective of the present study was to investigate the role of macrophagic autophagy after pulmonary exposure to CeO_2 NP in mice. To achieve our aim, mice lacking the early autophagy gene *Atg5* in their myeloid lineage and their wildtype counterparts were exposed to CeO_2 NP by single oropharyngeal administration and sacrificed up to one month after. At that time, lung remodeling was thoroughly characterized (inflammatory cells infiltration, expression of fibrotic markers such as αSMA, TGFβ1, total and type I and III collagen deposition), as well as macrophage infiltration (quantification and M1/M2 phenotype).

Results

Characterization of pulmonary remodeling in response to CeO_2 NP

Mice exposure to a single administration of 50 µg CeO_2 NP induced a profound lung fibrotic remodeling characterized by a progressive thickening of bronchiolar and alveolar walls. These modifications appeared gradually, starting from 24 hours post CeO_2 NP administration for bronchiolar modifications, and after 1 week for the alveolar ones (Fig. 1). They were accompanied by a persistent increased total cell count in the BAL (Fig. 1D). Cell differential analysis identified macrophages as the predominant cell population, with a transient significant increase of neutrophil percentage in BAL from CeO_2-exposed

animal 24 hours and 1 week after their initial exposure, but which was no more found after 1 month (Additional Fig. 1). As shown in Fig. 1E, CeO_2 NP were internalized in BAL macrophages at all time points.

To further characterize our model, we performed a dose-response experiment and analyzed the lung remodeling achieved in mice 28 days after exposure to one single administration of either 5 or 50 µg CeO_2 NP. As showed in Figs. 2 & 3, a significant thickening of alveolar and bronchiolar walls, together with a significant accumulation of total collagen, collagen I, collagen III, αSMA and TGF-ß in bronchiolar and alveolar area could be observed in mice exposed to 50 µg CeO_2 NP, while these effects where only intermediary in mice exposed to 5 µg CeO_2 NP (except for Collagen III alveolar deposition which was significatively different in mice exposed to 50 µg compared to Saline and 5 µg CeO_2 NP conditions). Quantification of Mac3 expression in lung tissue sections of CeO_2-exposed mice, as an index of total number of macrophages in lung tissue, confirmed the increased total number of macrophages observed in BAL, and demonstrated a predominant alveolar localization of macrophages in CeO_2-exposed animals, both in alveolar spaces as well as infiltrated in the interstitium (Fig. 4). As for BAL macrophages, CeO_2 NP were internalized in macrophages present in the alveolar area (Additional Fig. 1D).

Characterization of autophagy in response to CeO_2 NP exposure

To investigate whether autophagy was induced in our experimental model of lung fibrosis, we utilized GFP-LC3 transgenic mice and exposed them to 50 µg CeO_2 NP. As shown in Fig. 5, we were able to observe the induction of autophagy in CeO_2-exposed GFP-LC3 mice, already 24 h after the initial administration, and up to 28 days. This was observed mainly in epithelial cells in bronchiolar regions, and in macrophages in the alveoli (Fig. 5A-C). These results were confirmed by the observation of increased levels of Atg5 protein, an early marker of autophagy pathway, in similar regions of CeO_2-exposed mice, (Additional Fig. 2, Panel A).

As macrophages are supposedly important players in lung fibrosis (15), and as we recently demonstrated the importance of autophagy in macrophagic response to NP (14), we next focus our work on macrophages. The potential of CeO_2 NP to induce autophagy in macrophages was confirmed by the observed accumulation of GFP-LC3 puncta in peritoneal macrophages obtained from GFP-LC3 mice and exposed to CeO_2 NP in vitro (Fig. 5D), as well as by the induction of Atg5 protein expression in peritoneal macrophages of C57Bl/6 mice exposed to CeO_2 NP in vitro (Fig. 5E). Finally, as autophagy is a highly dynamic process, we addressed the issue of its activation in macrophages exposed to CeO_2 NP. As shown by Fig. 4F, we could observe the colocalization of LC3 staining with that of the lysosomal protein LAMP-1 in CeO_2 NP-exposed macrophages. Overall, these results indicate that pulmonary exposure to CeO_2 NP is followed by the activation of autophagy, especially in macrophages, which are able to phagocyte CeO_2 NP.

Effect of blockade of macrophagic autophagy in response to CeO_2 NP

In order to decipher the specific role of macrophagic autophagy in the development of lung fibrosis, mice lacking *Atg5* gene in their myeloid lineage ($Atg5^{flox/flox}$ $LysM^{Cre}$ or $Atg5^{+/-}$) were exposed to CeO_2 NP. These mice do not present any particular lung phenotype in absence of any exogenous exposure and their macrophages do not express Atg5 in response to CeO_2 NP (Additional Fig. 3). Twenty-eight days after the NP administration, histological analysis of lung tissue sections indicates that $Atg5^{+/-}$ mice present the same peribronchiolar fibrosis as compared to their wild type (WT) counterparts (Fig. 6, *: $p < 0.05$). In stark contrast, $Atg5^{+/-}$ mice were protected against CeO_2 NP-induced alveolar fibrosis; no alveolar wall thickening could be observed in these mice (Fig. 6 *: $p < 0.05$). This protection against alveolar remodeling was further confirmed by the quantification of total, type I and III collagen deposition, as well as expression of αSMA and TGF-ß: $Atg5^{+/-}$ mice present the same alveolar phenotype as their wild-type counterpart, whatever their exposure to CeO_2 NP (Fig. 7).

This protection wasn't the result of a differential CeO_2 NP accumulation between WT and $Atg5^{+/-}$ mice, as X-Ray microfluorescence(micro-XRF) showed that Ce signal could be observed with similar intensity whatever the mice genotype, mainly in the alveolar region, and much less in bronchiolar walls (Additional Fig. 4). Moreover, micro X-ray absorption near edge structure (XANES) spectra of Ce spots detected in CeO_2-exposed mice revealed three different types of modifications that could be observed: 1/ similar to that of the CeO_2 reference (red line in Additional Fig. 4E – Spectrum Type I); 2/ a spectrum presenting a shift of the first peak toward 5727 eV (instead of 5731 eV as in the reference – yellow line – Spectrum Type II), suggesting the reduction of Ce^{IV} to Ce^{III}; and 3/ a mixed contribution of Type I and Type II spectra (green line). A similar repartition of the different type of spectra could be observed in all CeO_2-exposed lungs, whatever the genotype (Table 2).

Table 2
Repartition of the different types of XANES spectra in WT and $Atg5^{+/-}$ samples

	Type I	Type II	Mix Type I + II
WT samples (%)	36.4	45,4	18.2
$Atg5^{+/-}$ samples (%)	33.3	48.2	18.5

Finally, the protection against alveolar fibrosis was the result of macrophage activity, as treatment of $Atg5^{+/-}$ mice with clodronate to remove macrophages completely abolished the protection against alveolar fibrosis observed in $Atg5^{+/-}$ mice, while no modification of bronchiolar fibrosis was observed (Additional Fig. 5 and data not shown).

Characterization of macrophage polarization in response to CeO_2 NP

Blockade of macrophagic autophagy didn't modify the increase in total number of macrophages induced by CeO_2 NP exposure (Fig. 8). However, when assessing the M1 or M2 phenotype of alveolar macrophages as potential contributors to alveolar fibrotic response (15), we observed that WT mice exposed to CeO_2 NP present an M1-like phenotype, with significantly increased expression of CD68, CD80 and iNOS proteins as compared to unexposed mice (Fig. 8C-E and 8I-K, *: $p < 0.005$), whereas *Atg5*$^{+/-}$ mice developed an M2-like phenotype, characterized by increased expression of CD206, CD163 and Arginase1 (Fig. 8F-H and 8L-N,*: $p < 0.005$). These results were confirmed in vitro; exposure of WT peritoneal macrophages to CeO_2 NP lead to the increased expression of M1 markers, while exposure of macrophages obtained from *Atg5*$^{+/-}$ mice lead to an increased expression of M2 markers (Additional Fig. 6).

Finally, this modification of macrophage polarization in *Atg5*$^{+/-}$ mice could be responsible of the protective effect against the development of alveolar fibrosis in *Atg5*$^{+/-}$ mice as exposure of WT fibroblasts to the supernatant of CeO_2-exposed macrophages induced fibroblast to myofibroblast differentiation, detected by an increased expression of αSMA, Collagen I and III, only when WT macrophages were used, but not macrophages bearing a *Atg5*$^{+/-}$ genotype (Fig. 9).

Discussion

Taken together, our results show the progressive and dose-dependent development of lung fibrosis in mice exposed to CeO_2 NP. They also demonstrate that the blockade of macrophagic autophagy protects from alveolar but not bronchiolar fibrosis, probably via the modulation of macrophage polarization in favor of a M2 phenotype.

The progressive and dose-dependent induction of pulmonary fibrosis that we describe here in response to CeO_2 NP single administration is in accordance with data from literature using other CeO_2 NP (1, 5–9). The same is true for the sustained pulmonary inflammation that we detected and which has been shown to be slow to resolve post exposure (16). We didn't however observe the formation of granuloma as described for example by Park and colleagues in CeO_2-exposed animals (8), but this is probably linked to the more relevant dose of CeO_2 NP that we used in our study; 5–50 µg per mouse versus 3 mg in Park study. Our results also confirm and extend the data obtained by Ma and colleagues, showing that rats exposure to CeO_2 NP lead to the induction of M1 phenotype in BAL macrophages of these animals (17). It must be noted however that 28 days after the initial administration, mRNA expression of Arginase 1 was increased in Park study, thus suggesting a shift toward M2 phenotype that was not observed in our WT animals, although care must be taken as only one single M2 marker was targeted in Park's work.

The development of bronchiolar fibrosis in response to CeO_2 NP was not prevented by the blockade of macrophagic autophagy. Interestingly, this could be paralleled by the very low Ce elemental signal observed by μXRF in bronchiolar regions, as well as the almost lack of macrophages present in these areas, suggesting that CeO_2-induced bronchiolar fibrosis is independent of macrophages. Although we did not investigate further the biological mechanism(s) underlying this bronchiolar fibrosis, the occurrence of epithelial-mesenchymal transition (EMT) could be an explanation. Indeed, Ma and colleagues have recently demonstrated that exposure to CeO_2 NP induces EMT in alveolar type II cells that ultimately plays a role in lung fibrosis (5). Similarly to what we have demonstrated with in vitro exposure of fibroblast to the supernatant of Ce-exposed macrophages, it could be interesting to explore the effect of the secretome from Ce-exposed epithelial cell on fibroblast to myofibroblast differentiation in our system.

The protection against alveolar fibrogenesis observed in Ce-exposed $Atg5^{+/-}$ mice could have been the result of decreased amounts of Ce present in alveolar regions of $Atg5^{+/-}$ mice. Indeed, autophagy is known to interplay with macrophage phagocytosis (18–20), and M2 polarization has been shown to enhance Si-NP uptake by macrophages (21). Although we did not strictly quantify the Ce content in WT and $Atg5^{+/-}$ mice exposed to CeO_2 NP, the similar μXRF signals obtained in both animal genotypes in terms of both intensity and tissue distribution, together with the similar total number of macrophages present in the lungs of WT and $Atg5^{+/-}$ animals strongly suggest that the protection against alveolar fibrosis observed in $Atg5^{+/-}$ animals is probably not the result of a decreased amount of CeO_2 NP in these individuals. CeO_2 is highly reactive, and it has been suggested that a change in the Ce^{3+}/Ce^{4+} ratio may play a significant role in toxicity determination (22), and could thus contribute to lung fibrosis development. In our experiment, while Ce in CeO_2 NP was Ce^{4+}, Ce in lung tissue was only 33–36% pure Ce^{4+}, indicating a change in speciation after NP administration. However, both WT and $Atg5^{+/-}$ mice showed a similar modification of their Ce speciation, with 45–48% as Ce^{3+}, and around 18% presenting a mix Ce^{3+}/Ce^{4+} form. Therefore, the specific protection against alveolar fibrosis observed in $Atg5^{+/-}$ mice could not be attributed to modifications of Ce speciation.

The modification of macrophage polarization related to their autophagy status could also represent an interesting candidate to explore the underlying mechanism that occurs in $Atg5^{+/-}$ mice (23). Indeed, macrophages are divided into two distinct sub-populations defined as classically activated pro-inflammatory M1 subtype and alternatively activated M2 subtype responsible for anti-inflammatory, tissue repair and remodeling (Novak and Koh 2013). Both M1 and M2 macrophages have been noted to be involved in the pathogenesis of pulmonary fibrosis, this translating the plasticity of macrophage polarization depending the micro-environment stimuli and signals (25). In our experimental model of lung fibrosis, we demonstrated that macrophages from autophagy-deficient mice tended to polarize into M2a and M2c phenotype whereas their wild-type counterparts exhibiting proficient autophagy skewed towards the M1 subtype. Interestingly, the induction of autophagy by advanced glycation end products or rapamycin triggered macrophage polarization toward M1 phenotype, as well as a sustained inflammation

in mice and patients, resulting in delayed wound healing. Moreover, the inhibition of autophagy reduced M1 population but no changes of M2 subtype, which is in accordance with our results (26). However, it must be noted that in mice under high fat diet, there was an increased M1 and decreased M2 polarization in macrophages with defective autophagy, leading to hepatic inflammation and the progression to liver injury (27). This underlines the importance of the environmental context in the overall autophagy effect, which could be a clue to the effects observed in our study, as to understand the underlying mechanism of macrophage specific polarization in absence of autophagy.

Finally, our results suggest that macrophagic autophagy can facilitate fibrosis. Although not in accordance with the initial acceptance that autophagy might be protective in lung fibrosis (11, 13, 28), our data are in line with more recent results from the literature showing an increased number of LC3-II puncta, an index of active autophagy, in fibroblast foci of patients with idiopathic pulmonary fibrosis (IPF), the most common form of pulmonary fibrosis (13, 29). In vitro, these authors also showed that autophagy is induced by TGFß, and that it is necessary for TGFß-induced fibrosis in both non-IPF and IPF fibroblasts (7). Interestingly, such a cell-specific role for autophagy has been recently described in chronic obstructive pulmonary disease (COPD) where autophagy is believed to be protective except in macrophages (10–12, 28). In lung fibrosis, the majority of the studies has focused on lung epithelial cells and/or fibroblasts (28), as the two major cell type involved in fibrogenesis (15). However, the recruitment of inflammatory cells, leading to the activation of effector cells, is often considered as a first trigger of fibrosis (30), and as such, the activation of macrophages occupies a pivotal role in the translation of injury to aberrant repair in lung fibrosis (31, 32). Interestingly, the LC3 puncta observed by Ghavami and colleagues in fibroblast foci of IPF patients are coherent with the presence of macrophages (29).

Conclusions

In conclusion, our finding bring novel insight on the role of macrophagic autophagy in lung fibrogenesis, and add to the current awareness of pulmonary macrophages as potential new therapeutic targets for future anti-fibrotic therapies (33).

Methods

Experimental model of lung fibrosis:

Eight to twelve weeks old C57Bl/6 mice received saline or CeO_2 NP (5 or 50 µg, NanoAmor, Houston, TX) via non-surgical oropharyngeal instillation (MicroSprayer® Aerosolizer, PennCentury). Mice were sacrificed 24 h, 1 or 4 weeks later. A broncho-alveolar lavage (BAL) was performed, and the lungs were harvested and collected for further analysis as previously described (34). A subset of mice were treated with Clodronate or liposome as negative control as previously described (35). Myeloid cell specific *Atg5* deficient mice ($Atg5^{fl/fl}$ LysM-$Cre^{+/-}$ mice further referred as $Atg5^{+/-}$) and their littermate wildtype (WT - $Atg^{fl/fl}$ LysM-$Cre^{-/-}$) counterpart were kindly provided by Fatima Clerc (36). GFP-LC3 mice were purchased

from Riken, Japan. The experimental protocol received the approval of the French Government (Ministère de l'Enseignement Supérieur, de la Recherche et de l'Innovation, APAFIS #14914-2018042515599016).

Histological and Immunohistochemistry analyses:

Paraffin embedded lung tissue sections (5 µM) were stained with Hematoxylin and Eosin or Sirius Red for histological observations and total collagen deposition, respectively. Immunohistochemistry experiments were performed using antibodies described in Table 1. At least 10 fields per lung tissue section (magnification 200X) were evaluated for the quantification of histological lesions and immunostainings using ImageJ software as previously described (34). Briefly, for alveolar wall thickening, alveolar images without bronchi were used to build a macro with threshold value for alveolar wall thickness excluding alveolar spaces. For bronchiolar thickening, at least 10 fields with well defined, large and round shaped bronchi were imaged per animal. The thickness of each individual bronchus was measured manually at four different regions in pixels, and the average pixels calculated from these regions was converted into µM for bronchiolar thickening.

Table 1
List of antibodies used in the study

Antibody	Dilution	Reference	Fabricant
Collagen 1	1:100	AB21286	Abcam, Cambridge, UK
Collagen 3	1:1000	AB7778	Abcam, Cambridge, UK
SMA	1:3000	AB5694	Abcam, Cambridge, UK
TGF-ß	1:100	PA5-86215	Thermo-Fisher, France
MAC3	1:50	550292	BD BioScience, France
CD68	1:100	AB125212	Abcam, Cambridge, UK
CD80	1:100	AB64116	Abcam, Cambridge, UK
iNOS	1:100	AB15323	Abcam, Cambridge, UK
CD163	1:250	AB182422	Abcam, Cambridge, UK
CD206	1:500	AB64693	Abcam, Cambridge, UK
Arginase-1	1:500	AB91279	Abcam, Cambridge, UK
LC3	1:1000	PM036	MBL International, MA
LAMP-1	1:50	AF4320	R&D Systems, France

For immunohistological analyses, a representative image of alveolar or bronchiolar regions was opened under ImageJ and zoomed in for 3 colors. The plug-in with color deconvolution was applied on the image followed by choosing of color 1 for DAB stain, color 2 for counter-stain, and color 3 for the white background. The next step was adjusting the threshold for 3 color regions and the specific threshold

values for each color were noted and close-all option was employed. The image was then opended and plugin-macro-record and plugin-color deconvolution were applied to the image step-wise. Threshold was adjusted, and the noted values for color 2 and color 1 were set for analyzing the measure for each color.

Lung primary cells culture

Peritoneal macrophages: Primary cultures of peritoneal macrophages were obtained as previously described (37). Briefly, 2 ml of sterile 4% thioglycolate broth (T0157, Sigma-Aldrich, La Verpillère, France) were administered in the peritoneal cavity of C57Bl/6 mice. Seventy-two hours later, peritoneal macrophages were harvested from the peritoneal cavity and cultured in DMEM medium, supplemented with 10% fetal bovine serum (FBS) and 1% penicillin/streptomycin. For immunocytochemistry experiments, cells were seeded in 8-well cell culture chamber slides (LabTek, Nunc, ATGC Biotechnology, France) and exposed for 24 hours to 10 µg/ml CeO_2 NP. After incubation with the primary antibody of interest (Table 1), cells were labelled with secondary antibodies: Alexa Fluor 488 (green) for LC3 and Alexa Fluor 546 (red) for LAMP1. The fluorescence images were captured using Zeiss LSM-510 multitracking laser scanning confocal microscope with a Helium/Neon laser at 543 nm and using AxioVision software (Carl Zeiss).

Lung fibroblasts: Primary fibroblasts cells were isolated from mouse lungs by mechanic dissection and enzymatic digestion (collagenase 4,1% in HBSS). They were maintained in Dulbecco's modified Eagle's medium (DMEM) and Glutamax (Gibco, 31966-021) containing 10% foetal bovine serum (Eurobio) and streptomycin penicillin (Life Technologies, E1740384 100 µg/ml).

X-ray microfluorescence experiments:

The localization and speciation of Ce in the lungs were assessed on lung tissue sections embedded in paraffin, using X-ray microfluorescence (micro-XRF) and micro X-ray absorption near edge structure (micro-XANES) as previously described (34). These experiments were performed at the LUCIA beamline of the SOLEIL synchrotron (Orsay, France – (38, 39)). A total of 29 spectra in WT and 22 spectra in $Atg5^{+/-}$ animals have been recorded.

Statistical analysis:

At least five mice per experimental group were utilized. Taking into account the possibility of non-normal distribution in the mice population, nonparametric tests (Kruskal–Wallis statistical test followed by Dunn's multiple comparison test) were used (40). Values are expressed as the mean ± SEM. Data were analyzed with GraphPad Prism 6.0 (La Jolla, CA) and STATA v13.0 (College Station, TX). For all statistical tests, p values smaller than 0.05 were considered as significant.

Abbreviations

BAL
broncho-alveolar lavage

CeO_2
Cerium Oxide
FBS
Fetal Bovine Serum
µXANES
Micro X-ray absorption near edge structure
µXRF
X-ray microfluorescence
NP
nanoparticles
REE
rare earth elements

Declarations

Ethical approval and Consent to participate:

The experimental protocol received the approval of the French Government (Ministère de l'Enseignement Supérieur, de la Recherche et de l'Innovation, APAFIS #14914-2018042515599016).

Consent for publication:

Not applicable.

Availability of data and materials:

The datasets used and/or analysed during the current study are available from the corresponding author on reasonable request.

Competing interests:

No competing interest to declare.

Funding:

This work was supported by a funding of the French "Investissement d'Avenir" program LabEx SERENADE project (B. Annangi recipient of Research Chair).

Author's contributions:

BA contributed to the design of experimental work, acquisition and analysis of data, and wrote the first draft of the manuscript. ZL, JBr, AR and VMS contributed to acquisition of data, DV contributed to acquisition and analysis of data, JBo critically revised the manuscript, and SL designed the work and critically wrote and revised the manuscript.

Acknowledgements:

Authors wish to acknowledge the expertise of Erwan Paineau for the μXRF analyses, and the expert advises of Fatima Clerc on $Atg5^{+/-}$ mice.

Authors' information: Not applicable.

References

1. Gwenzi W, Mangori L, Danha C, Chaukura N, Dunjana N, Sanganyado E. Sources, behaviour, and environmental and human health risks of high-technology rare earth elements as emerging contaminants. Sci Total Environ [Internet]. 2018/05/02. 2018 Sep;636:299–313. Available from: https://linkinghub.elsevier.com/retrieve/pii/S0048969718314128
2. Cassee FR, van Balen EC, Singh C, Green D, Muijser H, Weinstein J, et al. Exposure, health and ecological effects review of engineered nanoscale cerium and cerium oxide associated with its use as a fuel additive. Crit Rev Toxicol [Internet]. 2011;41(3):213–29. Available from: https://www.ncbi.nlm.nih.gov/pubmed/21244219
3. Pairon JC, Roos F, Iwatsubo Y, Janson X, Billon-Galland MA, Bignon J, et al. Lung retention of cerium in humans. Occup Environ Med. 1994;
4. Porru S, Placidi D, Quarta C, Sabbioni E, Pietra R, Fortaner S. The potencial role of rare earths in the pathogenesis of interstitial lung disease: A case report of movie projectionist as investigated by neutron activation analysis. J Trace Elem Med Biol. 2001;
5. Ma J, Bishoff B, Mercer RR, Barger M, Schwegler-Berry D, Castranova V. Role of epithelial-mesenchymal transition (EMT) and fibroblast function in cerium oxide nanoparticles-induced lung fibrosis. Toxicol Appl Pharmacol. 2017/03/21. 2017;323:16–25.
6. Ma JY, Mercer RR, Barger M, Schwegler-Berry D, Scabilloni J, Ma JK, et al. Induction of pulmonary fibrosis by cerium oxide nanoparticles. Toxicol Appl Pharmacol [Internet]. 2012;262(3):255–64. Available from: https://www.ncbi.nlm.nih.gov/pubmed/22613087
7. Ma JY, Young SH, Mercer RR, Barger M, Schwegler-Berry D, Ma JK, et al. Interactive effects of cerium oxide and diesel exhaust nanoparticles on inducing pulmonary fibrosis. Toxicol Appl Pharmacol [Internet]. 2014;278(2):135–47. Available from: https://www.ncbi.nlm.nih.gov/pubmed/24793434
8. Park E-J, Cho W-S, Jeong J, Yi J, Choi K, Kim Y, et al. Induction of Inflammatory Responses in Mice Treated with Cerium Oxide Nanoparticles by Intratracheal Instillation. J Heal Sci [Internet]. 2010;56(4):387–96. Available from: http://joi.jlc.jst.go.jp/JST.JSTAGE/jhs/56.387?from=CrossRef

9. Guo C, Robertson S, Weber RJM, Buckley A, Warren J, Hodgson A, et al. Pulmonary toxicity of inhaled nano-sized cerium oxide aerosols in Sprague–Dawley rats. Nanotoxicology. 2019 Jul 3;13(6):733–50.
10. Dikic I, Elazar Z. Mechanism and medical implications of mammalian autophagy. Nat Rev Mol Cell Biol. 2018/04/06. 2018;19(6):349–64.
11. Nakahira K, Pabon Porras MA, Choi AMK. Autophagy in Pulmonary Diseases. Am J Respir Crit Care Med [Internet]. 2016; Available from: http://dx.doi.org/10.1164/rccm.201512-2468SO
12. Racanelli AC, Kikkers SA, Choi AMK, Cloonan SM. Autophagy and inflammation in chronic respiratory disease. Autophagy [Internet]. 2018;14(2):221–32. Available from: https://doi.org/10.1080/15548627.2017.1389823
13. Patel AS, Lin L, Geyer A, Haspel JA, An CH, Cao J, et al. Autophagy in idiopathic pulmonary fibrosis. PLoS One [Internet]. 2012/07/21. 2012;7(7):e41394. Available from: http://www.ncbi.nlm.nih.gov/entrez/query.fcgi?cmd=Retrieve&db=PubMed&dopt=Citation&list_uids=22815997
14. Cohignac V, Landry MJ, Ridoux A, Pinault M, Annangi B, Gerdil A, et al. Carbon nanotubes, but not spherical nanoparticles, block autophagy by a shape-related targeting of lysosomes in murine macrophages. Autophagy. 2018;14(8).
15. Wynn TA, Vannella KM. Macrophages in Tissue Repair, Regeneration, and Fibrosis. Immunity [Internet]. 2016;44(3):450–62. Available from: http://www.sciencedirect.com/science/article/pii/S107476131630053X
16. Aalapati S, Ganapathy S, Manapuram S, Anumolu G, Prakya BM. Toxicity and bio-accumulation of inhaled cerium oxide nanoparticles in CD1 mice. Nanotoxicology [Internet]. 2014;8(7):786–98. Available from: http://informahealthcare.com/doi/abs/10.3109/17435390.2013.829877
17. Ma JY, Zhao H, Mercer RR, Barger M, Rao M, Meighan T, et al. Cerium oxide nanoparticle-induced pulmonary inflammation and alveolar macrophage functional change in rats. Nanotoxicology. 2011 Sep;5(3):312–25.
18. Zhu Y, Li H, Ding S, Wang Y. Autophagy inhibition promotes phagocytosis of macrophage and protects mice from methicillin-resistant staphylococcus aureus pneumonia. J Cell Biochem. 2018/01/19. 2018;119(6):4808–14.
19. Germic N, Frangez Z, Yousefi S, Simon HU. Regulation of the innate immune system by autophagy: monocytes, macrophages, dendritic cells and antigen presentation. Cell Death Differ. 2019/02/10. 2019;26(4):715–27.
20. Bonilla DL, Bhattacharya A, Sha Y, Xu Y, Xiang Q, Kan A, et al. Autophagy regulates phagocytosis by modulating the expression of scavenger receptors. Immunity. 2013/09/17. 2013;39(3):537–47.
21. Hoppstädter J, Seif M, Dembek A, Cavelius C, Huwer H, Kraegeloh A. M2 polarization enhances silica nanoparticle uptake by macrophages. Front Pharmacol [Internet]. 2015;6. Available from: http://dx.doi.org/10.3389/fphar.2015.00055

22. Auffan M, Rose J, Orsiere T, De Meo M, Thill A, Zeyons O, et al. CeO2 nanoparticles induce DNA damage towards human dermal fibroblasts in vitro. Nanotoxicology. 2009 Jun;3(2):161–71.
23. Chen P, Cescon M, Bonaldo P. Autophagy-mediated regulation of macrophages and its applications for cancer. Autophagy. 2013/12/05. 2014;10(2):192–200.
24. Novak ML, Koh TJ. Macrophage phenotypes during tissue repair. J Leukoc Biol [Internet]. 2013;93(6):875–81. Available from: http://www.jleukbio.org/content/93/6/875.abstract
25. Zhang L, Wang Y, Wu G, Xiong W, Gu W, Wang CY. Macrophages: Friend or foe in idiopathic pulmonary fibrosis? Respiratory Research. 2018.
26. Guo Y, Lin C, Xu P, Wu S, Fu X, Xia W, et al. AGEs Induced Autophagy Impairs Cutaneous Wound Healing via Stimulating Macrophage Polarization to M1 in Diabetes. Sci Rep. 2016/11/03. 2016;6:36416.
27. Liu K, Zhao E, Ilyas G, Lalazar G, Lin Y, Haseeb M, et al. Impaired macrophage autophagy increases the immune response in obese mice by promoting proinflammatory macrophage polarization. Autophagy [Internet]. 2015;11(2):271–84. Available from: https://www.ncbi.nlm.nih.gov/pubmed/25650776
28. Hill C, Li J, Liu D, Conforti F, Brereton CJ, Yao L, et al. Autophagy inhibition-mediated epithelial-mesenchymal transition augments local myofibroblast differentiation in pulmonary fibrosis. Cell Death Dis. 2019/08/09. 2019;10(8):591.
29. Ghavami S, Yeganeh B, Zeki AA, Shojaei S, Kenyon NJ, Ott S, et al. Autophagy and the unfolded protein response promote profibrotic effects of TGF-beta1 in human lung fibroblasts. Am J Physiol Lung Cell Mol Physiol. 2017/10/28. 2018;314(3):L493-l504.
30. Rockey DC, Bell PD, Hill JA. Fibrosis–a common pathway to organ injury and failure. N Engl J Med. 2015/03/19. 2015;372(12):1138–49.
31. O'Dwyer DN, Ashley SL, Moore BB. Influences of innate immunity, autophagy, and fibroblast activation in the pathogenesis of lung fibrosis. Am J Physiol Lung Cell Mol Physiol. 2016/07/31. 2016;311(3):L590-601.
32. Venosa A, Malaviya R, Gow AJ, Hall L, Laskin JD, Laskin DL. Protective role of spleen-derived macrophages in lung inflammation, injury, and fibrosis induced by nitrogen mustard. Am J Physiol Lung Cell Mol Physiol. 2015/10/18. 2015;309(12):L1487-98.
33. Byrne AJ, Maher TM, Lloyd CM. Pulmonary Macrophages: A New Therapeutic Pathway in Fibrosing Lung Disease? Trends Mol Med [Internet]. 2016/03/17. 2016;22(4):303–16. Available from: https://www.ncbi.nlm.nih.gov/pubmed/26979628
34. Paul E, Franco-Montoya M-L, Paineau E, Angeletti B, Vibhushan S, Ridoux A, et al. Pulmonary exposure to metallic nanomaterials during pregnancy irreversibly impairs lung development of the offspring. Nanotoxicology. 2017;11(4).
35. Seki E, De Minicis S, Osterreicher CH, Kluwe J, Osawa Y, Brenner DA, et al. TLR4 enhances TGF-beta signaling and hepatic fibrosis. Nat Med [Internet]. 2007/10/24. 2007;13(11):1324–32. Available

from: http://www.ncbi.nlm.nih.gov/entrez/query.fcgi?cmd=Retrieve&db=PubMed&dopt=Citation&list_uids=17952090

36. Lodder J, Denaes T, Chobert MN, Wan J, El-Benna J, Pawlotsky JM, et al. Macrophage autophagy protects against liver fibrosis in mice. Autophagy [Internet]. 2015;11(8):1280–92. Available from: http://www.ncbi.nlm.nih.gov/pubmed/26061908
37. Zhang X, Goncalves R, Mosser DM. The isolation and characterization of murine macrophages. Vol. CHAPTER, Current Protocols in Immunology. NIH Public Access; 2008. p. Unit.
38. Vantelon D, Trcera N, Roy D, Moreno T, Mailly D, Guilet S, et al. The LUCIA beamline at SOLEIL. J Synchrotron Radiat. 2016;
39. Flank AM, Cauchon G, Lagarde P, Bac S, Janousch M, Wetter R, et al. LUCIA, a microfocus soft XAS beamline. Nucl Instruments Methods Phys Res Sect B Beam Interact with Mater Atoms. 2006;
40. Weissgerber TL, Milic NM, Winham SJ, Garovic VD. Beyond bar and line graphs: time for a new data presentation paradigm. PLoS Biol [Internet]. 2015;13(4):e1002128. Available from: https://www.ncbi.nlm.nih.gov/pubmed/25901488

Figures

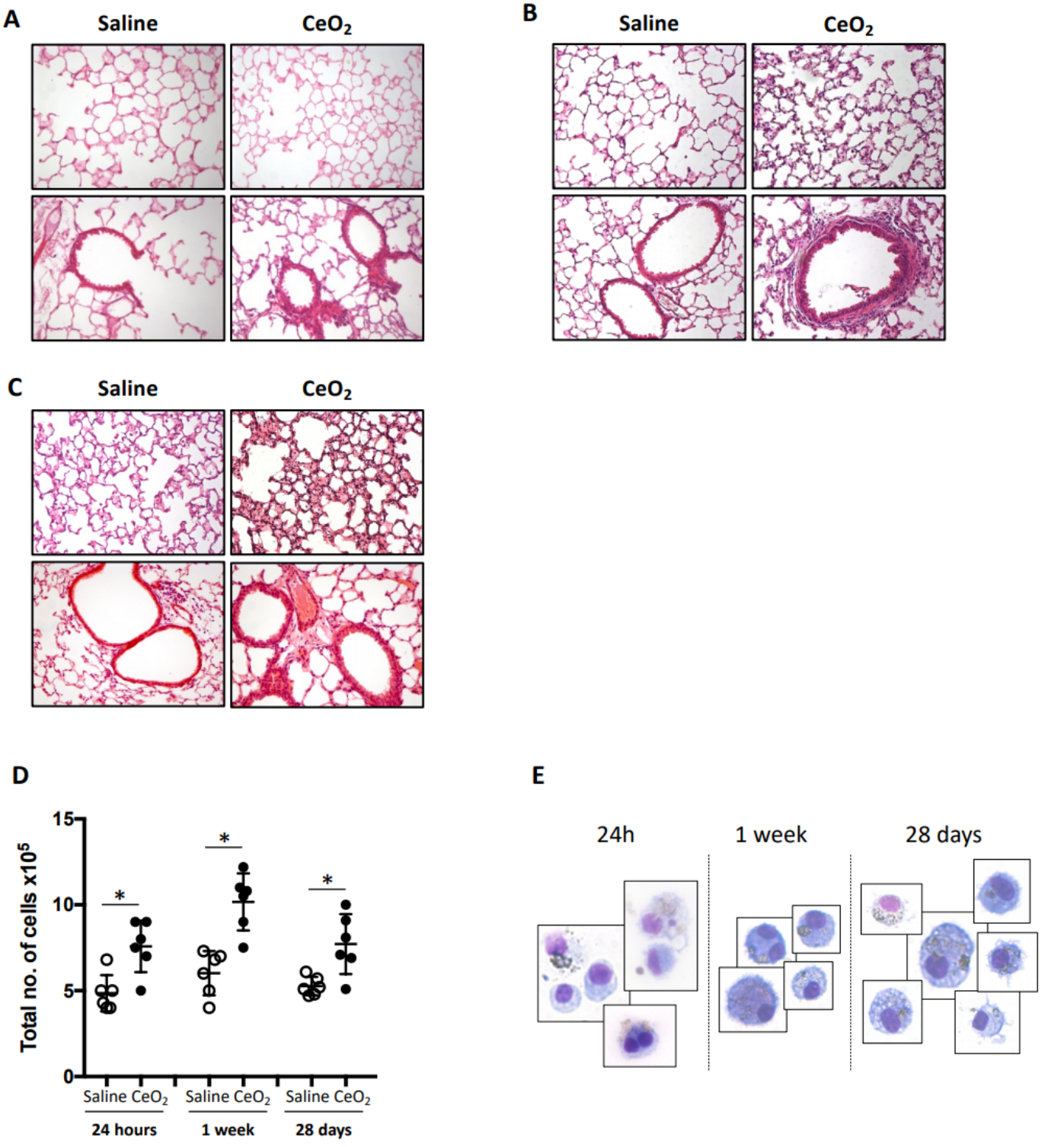

Figure 1

Exposure to CeO2 NP induces a progressive lung remodeling Representative lung tissue sections of mice exposed to Saline or CeO2 NP and stained with Hematoxylin Eosin (HE) after 1 day (Panel A), 7 days (Panel B) or 28 days (Panel C). Original magnification x200. Quantification of total cell count in BAL fluid (Panel D). Each individual circle represents the value obtained from one animal (empty circle: saline

exposure – plain circle: CeO2 NP-exposure). *p<0.05. Typical images of BAL macrophages with internalized NP (Panel E).

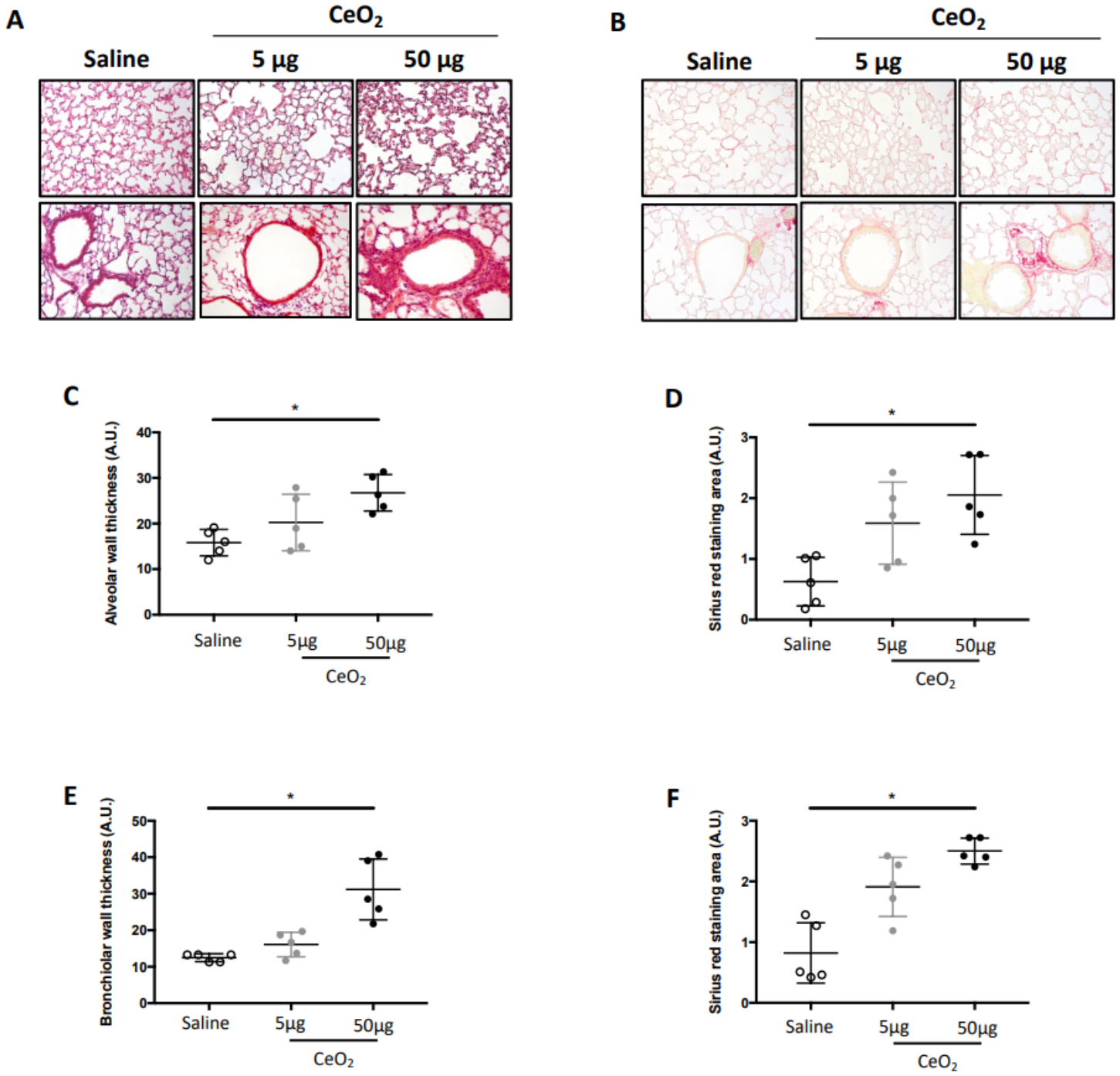

Figure 2

Exposure to CeO2 NP induces a dose-dependent lung remodeling in mice Representative lung tissue sections of mice exposed to Saline, 5 or 50 µg CeO2 NP and stained, after 28 days, for Hematoxylin Eosin (Panel A) or PicroSirius Red (Panel B). Original magnification x200. Quantification of alveolar wall (Panel C) or bronchiolar wall (Panel E) thickness (Panel C and E) and total collagen deposition (Panel D and F).

Each individual circle represents the mean value obtained from one animal. Empty circle: saline exposure. Grey circle: 5µg CeO2 NP exposure. Plain circle: 50 µg CeO2 NP exposure. *p<0.05.

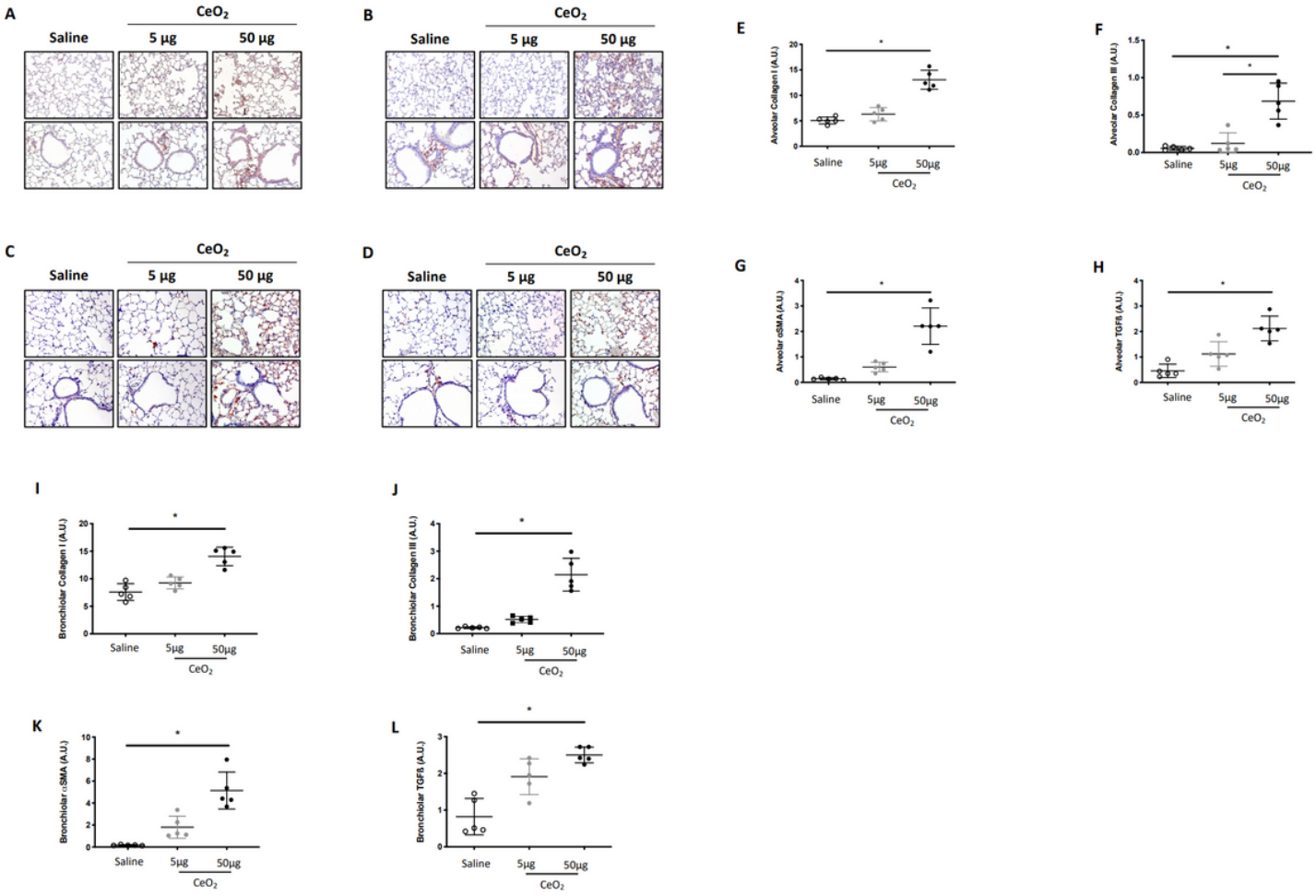

Figure 3

Characterization of the dose-dependent CeO2-induced lung fibrosis at 28 days Representative lung tissue sections of mice exposed to Saline or CeO2 NP (5 or 50µg) and stained with Collagen type I (Panel A), Collagen type III (Panel B), SMA (Panel C) and TGF-ß (Panel D). Original magnification x200. Quantification of Collagen I (alveolar - Panel E, bronchiolar - Panel I), Collagen III (alveolar - Panel F, bronchiolar - Panel J), SMA (alveolar - Panel G, bronchiolar - Panel K) and TGF-ß (alveolar - Panel H, bronchiolar - Panel L) respective area. Each individual symbol represents the value obtained from one animal (legend as in Figure 2). *p<0.05.

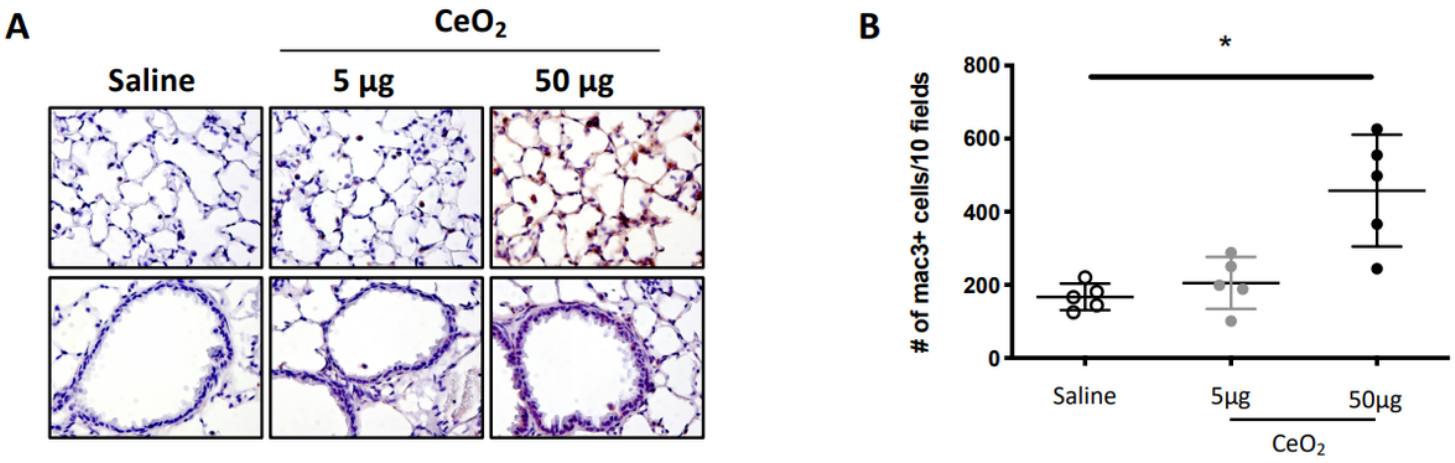

Figure 4

Exposure to CeO2 NP induces macrophage recruitment Representative lung tissue sections of mice exposed to Saline or CeO2 NP (5 or 50µg), after immunostaining for Mac3, as a marker of total number of macrophages (Panel A). Original magnification x200. Quantification of Mac3 positive cells (Panel B). Legend as in Figure 2.

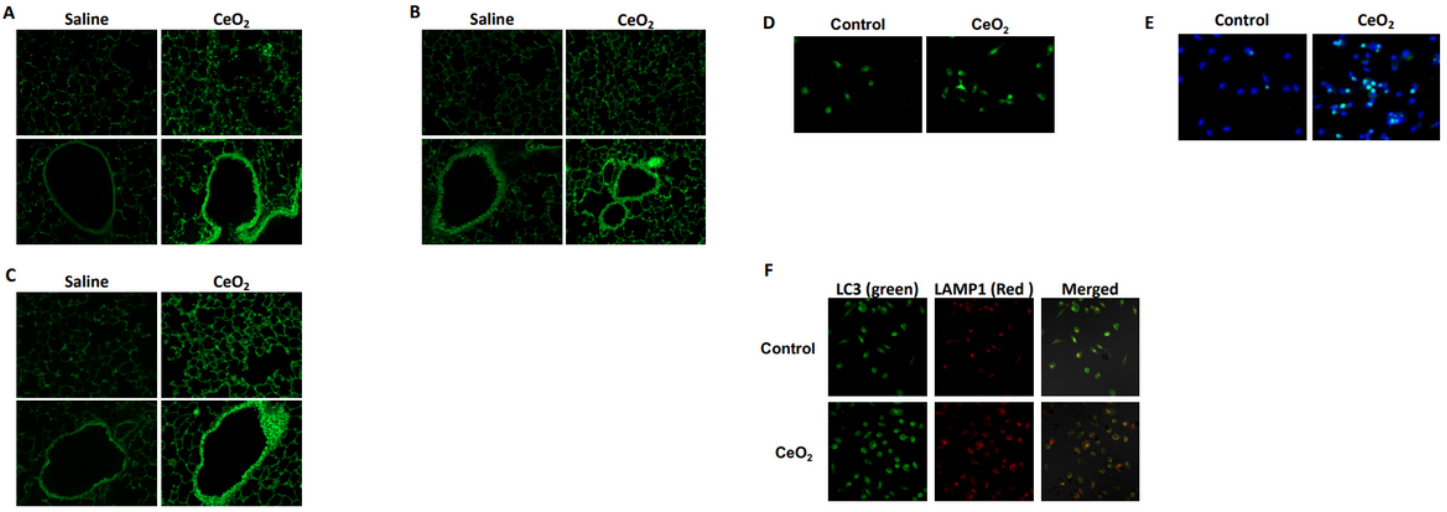

Figure 5

Exposure to CeO2 NP induces autophagy Representative lung tissue sections of GFP-LC3 mice exposed to Saline or CeO2 NP after 1 day (Panel A), 7 days (Panel B) or 28 days (Panel C). Original magnification x200. Panel D: Peritoneal macrophages of GPF-LC3 mice exposed to vehicle (Control) or 10 µg/ml CeO2 NP (CeO2). Panel E: expression of Atg5 in peritoneal macrophages form CeO2-exposed mice. Panel F: colocalization of LC3 (green) and LAMP1 (red) expression in mouse peritoneal macrophages in response to vehicle or CeO2 NP.

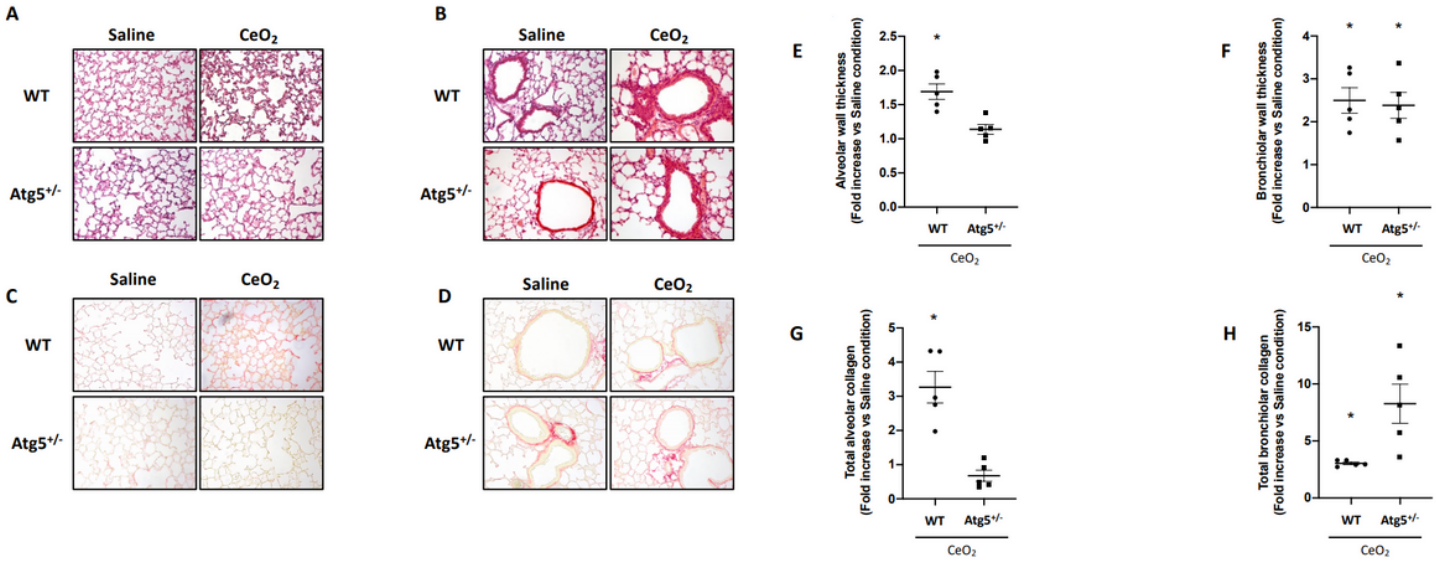

Figure 6

Atg5+/- mice are protected from alveolar remodeling Representative lung tissue sections of WT and Atg5+/- mice exposed to Saline or CeO2 NP, with a focus on alveolar (Panel A and C) or bronchiolar (Panel B and D) regions, after HES (Panel A and B) or Sirius red (Panel C and D) staining. Quantification of alveolar wall (Panel E) or bronchiolar wall (Panel F) thickness, and total alveolar (Panel G) or bronchiolar (Panel H) collagen deposition. Results are expressed as fold increase versus Saline condition. Circle: WT animals. Square: Atg5+/- animals. *p<0.05.

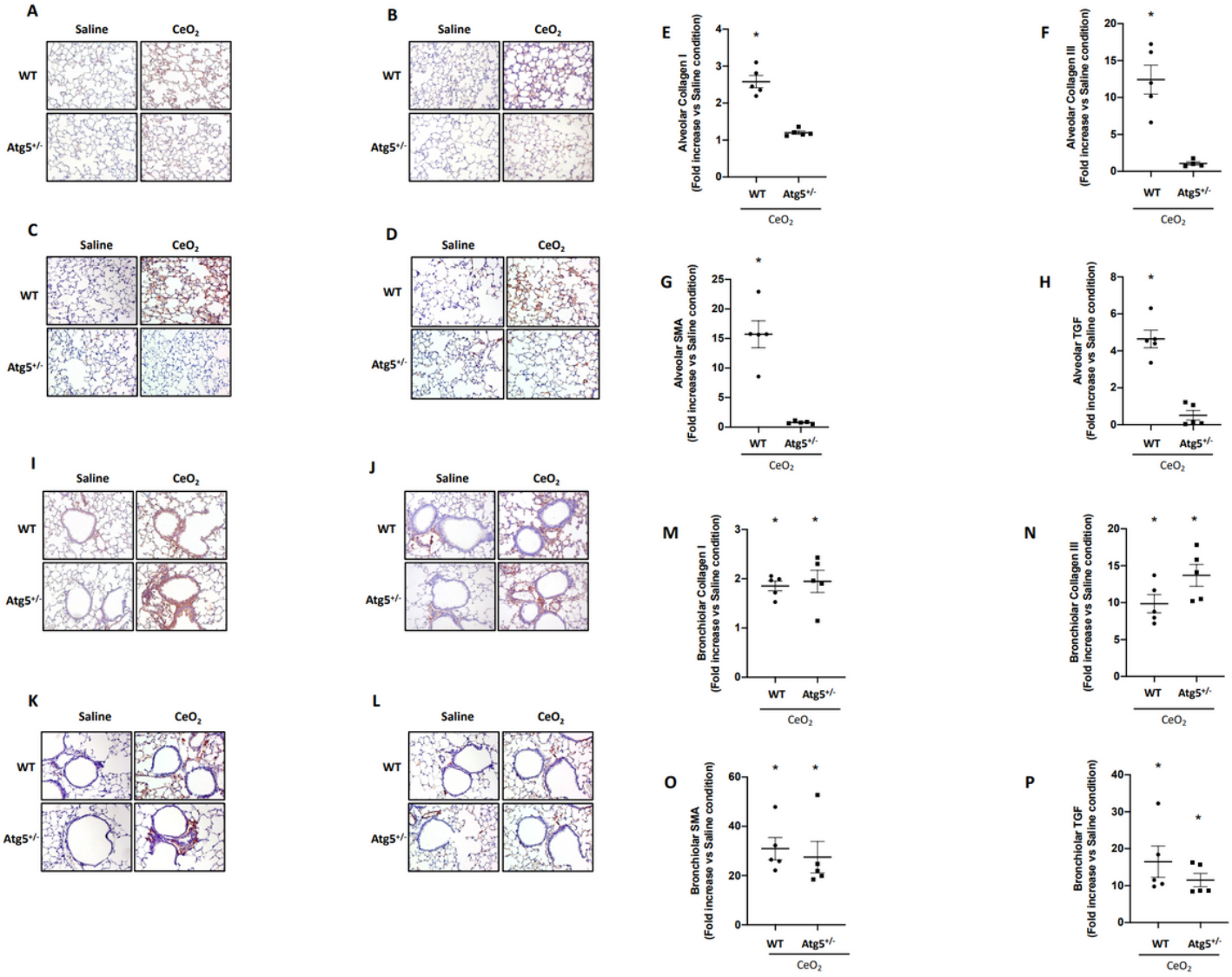

Figure 7

Characterization of lung remodeling in Atg5+/- mice Representative lung tissue sections of WT and Atg5+/- mice exposed to Saline or CeO2 NP, after (immune)stained with Collagen type I (Panel A and I), Collagen type III (Panel B and J), SMA (Panel C and K) and TGF-ß (Panel D and L). Original magnification x200. Quantification of Collagen I (alveolar - Panel E, bronchiolar - Panel M), Collagen III (alveolar - Panel F, bronchiolar - Panel N), SMA (alveolar - Panel G, bronchiolar - Panel O) and TGF-ß (alveolar - Panel H, bronchiolar - Panel P) respective area. Results are expressed as fold increase versus Saline condition. Circle: WT animals. Square: Atg5+/- animals. *p<0.05.

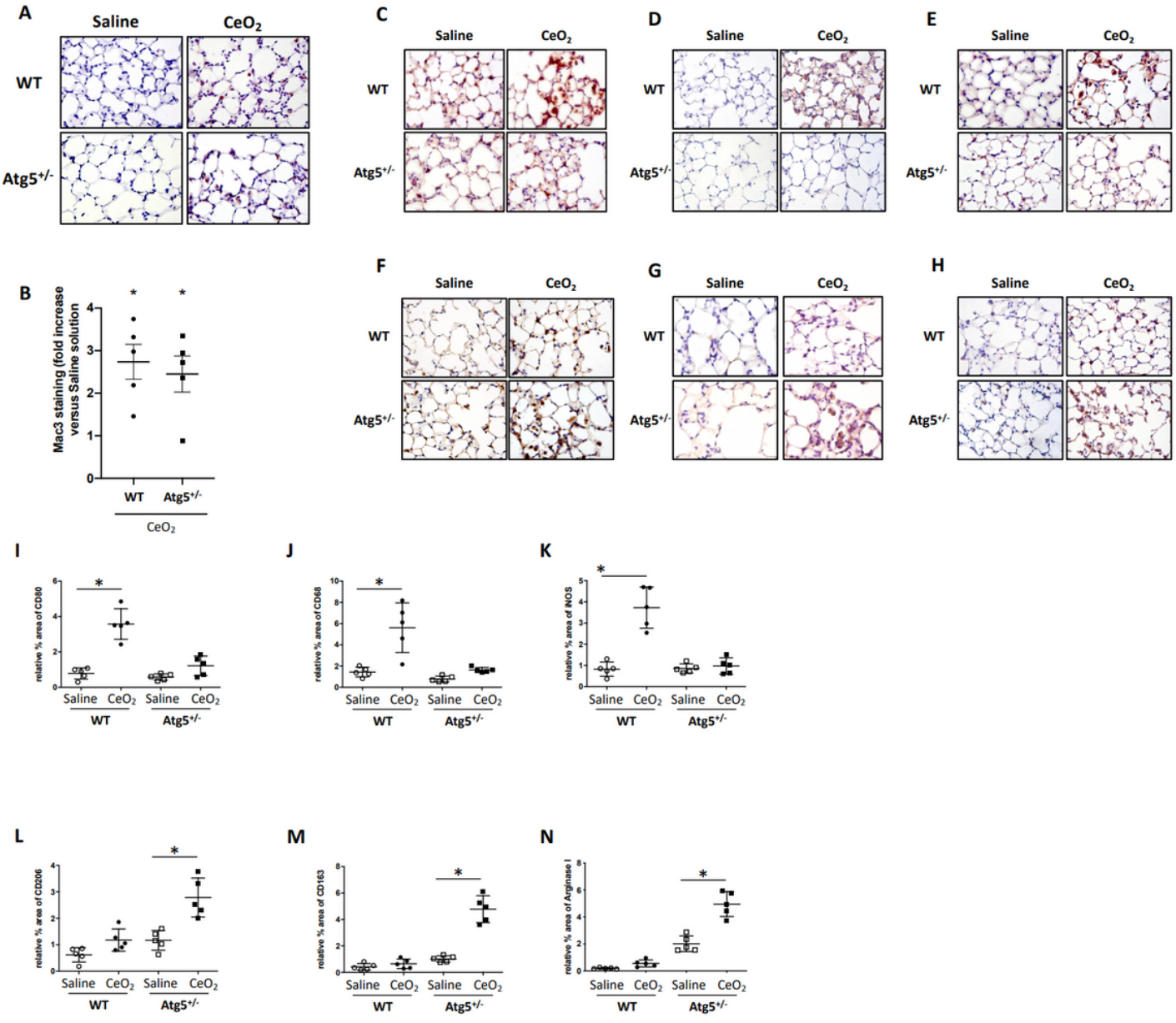

Figure 8

Characterization of CeO2-induced macrophage polarization in mice Representative lung tissue sections of mice exposed to Saline or CeO2 NP (5 or 50µg), after immunostaining for Mac3, as a marker of total number of macrophages (Panel A), CD80 (Panel C), CD68 (Panel D), iNOS (Panel E), CD206 (Panel F), CD163 (Panel G) or Arginase 1 (Panel H). Original magnification x200. Quantification of Mac3 positive cells (Panel B), CD80 (Panel I), CD68 (Panel J), iNOS (Panel K), CD206 (Panel L), CD163 (Panel M) or Arginase 1 (Panel N) respective area. Results are expressed as fold increase versus Saline condition. Circle: WT animals. Square: Atg5+/- animals. *p<0.05.

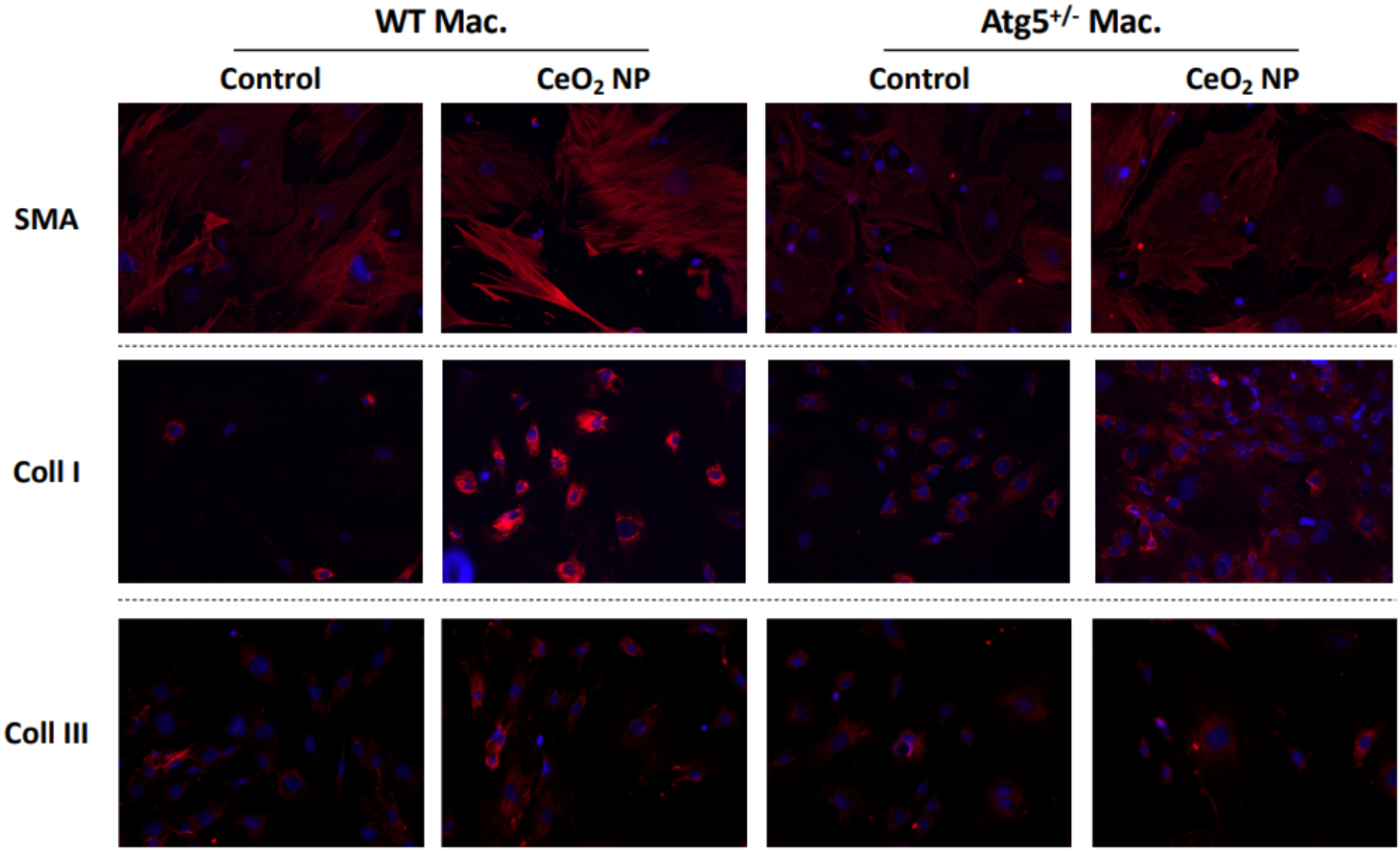

Figure 9

Fibroblast differentiation in vitro Representative images of WT fibroblasts exposed to supernatant of Vehicle (Control) or CeO2 NP-exposed macrophages obtained from WT of Atg5+/- mice, and immuno-stained for SMA, Collagen type I or type III.

Supplementary Files

This is a list of supplementary files associated with this preprint. Click to download.

- AdditionalFigure6.pdf
- AdditionalFigure5.pdf
- AdditionalFigure4.pdf
- AdditionalFigure3.pdf
- AdditionalFigure2.pdf
- AdditionalFigure1.pdf